Dynamics of an Algae-Bacteria Microcosm: Photosynthesis, Chemotaxis, and Expulsion in Inhomogeneous Active Matter

Praneet Prakash[a,1], **Yasa Baig**[a,1], **François J. Peaudecerf**[b], **and Raymond E. Goldstein**[a,2]

This manuscript was compiled on May 21, 2024

In Nature there are significant relationships known between microorganisms from two kingdoms of life, as in the supply of vitamin B_{12} by bacteria to algae. Such interactions motivate general investigations into the spatio-temporal dynamics of metabolite exchanges. Here we study by experiment and theory a model system: a coculture of the bacterium *B. subtilis*, an obligate aerobe that is chemotactic to oxygen, and a nonmotile mutant of the alga *C. reinhardtii*, which photosynthetically produces oxygen when illuminated. Strikingly, when a shaft of light illuminates a thin, initially uniform suspension of the two, the chemotactic influx of bacteria to the photosynthetically active region leads to expulsion of the algae from that area. We propose that this effect arises from advection by the inhomogeneous bacterial concentration. The resulting generalization of Fick's law has been proposed in the context of chemotaxis, and is mathematically related to the "turbulent diamagnetism" associated with magnetic flux expulsion in stars.

Active Matter | Chemotaxis | Photosynthesis

Significance Statement

Symbiotic relationships between photosynthetic algae and bacteria are known to be important in a variety of natural habitats, but the spatio-temporal aspects of such interactions are poorly understood. Here we explore by experiment and theory a realization of these interactions in which chemotactic bacteria respond to the oxygen produced by immotile green algae through photosynthesis. When the illumination triggering the photosynthesis is a circular shaft of light we find the surprising result that the chemotactic influx of bacteria ultimately results in the expulsion of algae. In developing a mathematical model of this behavior it is necessary to consider a generalization of Fick's law of diffusion that incorporates the effects of an inhomogeneous bacterial concentration on the transport of algae.

In the early 1880s the biologist Theodor Engelmann performed experiments that were perhaps the first to use bacteria as sensors (1–3). Several years prior he made the first observation of bacterial chemotaxis toward oxygen, by showing that putrefactive bacteria would migrate toward the chloroplasts of the filamentous alga *Spirogyra*. He then determined the "action spectrum" of photosynthesis—the wavelength-dependent rate of photosynthetic activity—by passing sunlight through a prism and projecting the spectrum onto a filamentous green algae held in a chamber that contained those self-same bacteria, which gathered around the algae in proportion to the local oxygen concentration, providing a direct readout of the oxygen production rate.

Although Engelmann's system was engineered for a particular purpose, and at first glance involves a *one-way* exchange of oxygen for the benefit of bacteria, there are many examples of mutualistic exchanges between microorganisms from two kingdoms of life. One of considerable significance is that involving vitamin B_{12}. In a landmark study (4), it was shown that a significant fraction of green algae that require this vitamin for their metabolism do not produce it, and as the ambient concentration of B_{12} in the aqueous environment is so low, they instead acquire it from a mutualistic relationship with bacteria, which benefit from carbon source.

The study of B_{12} transfer raises fascinating questions in biological physics related to the interplay of metabolite production, chemotaxis, and growth (5), including the issue of how organisms find each other (6) and stay together in the turbulent environment of the ocean, and how advection by fluid flows arising from microorganism motility affects such mutualisms. As it is difficult to control the production of vitamin B_{12}, we sought to construct a system in which the production of a chemical species needed by one member of an interacting pair of organisms could be controlled by the experimentalist. Taking motivation both from Engelmann's experiments and the B_{12} system, we introduce here a coculture (7) in which an obligate aerobic bacterium (one that requires oxygen) that is chemotactic toward oxygen coexists with a green alga whose photosynthetic activity can be turned on and off simply by controlling the external illumination. We use the bacterium *Bacillus subtilis*, whose aerotaxis has been central in the study of bioconvection (8) and in the discovery of "bacterial turbulence" (9), the dynamical state of a concentrated suspension with transient, recurring vortices and jets of collective swimming on scales large compared to the individual bacteria. The alga species is the well-studied unicellular *Chlamydomonas reinhardtii*, a model organism for biological fluid dynamics (10) with readily available motility mutants

Author affiliations: [a]Department of Applied Mathematics and Theoretical Physics, Centre for Mathematical Sciences,, University of Cambridge, Wilberforce Road, Cambridge CB3 0WA, United Kingdom; [b]Institute de Physique de Rennes, Universite Rennes, UMR 6251, F-35000 Rennes, France

P.P., Y.B., F.J.P. and R.E.G. designed research; P.P., Y.B., F.J.P. and R.E.G. performed research; P.P., Y.B., F.J.P. and R.E.G. analyzed data; and P.P., Y.B., and R.E.G. wrote the paper.

The authors declare no competing interests.

[1] P.P. and Y. B. contributed equally to this work.

[2]To whom correspondence should be addressed. E-mail: R.E.Goldstein@damtp.cam.ac.uk.

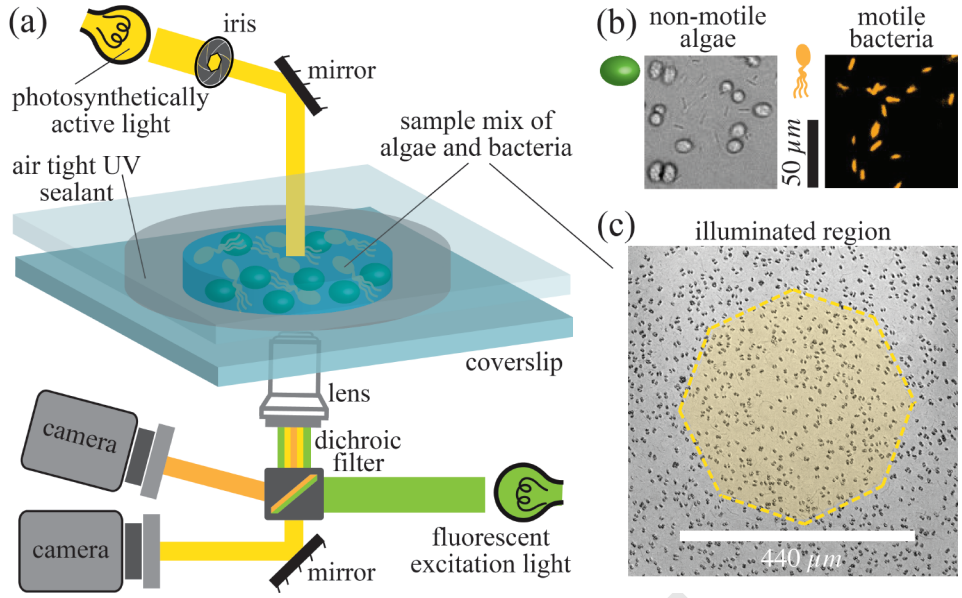

Fig. 1. Experimental setup. (a) Schematic of system to illuminate a coculture of a fluorescent strain of the bacterium *B. subtilis* and a flagella-less mutant of the green alga *C. reinhardtii*, initially distributed uniformly within the sample chamber. After a shaft of visible light illuminates the central region the algae produce oxygen to which the bacteria are attracted. (b) Algae and bacteria as observed through the brightfield and fluorescent channels, respectively. (c) Yellow shading indicates the illuminated region of the sample chamber, with dark algae visible in the background.

useful in probing the role of swimming in metabolite transfer. Together these define what we term the *algae-bacteria-chemoattractant system* (ABC). While coupled population dynamics problems have been studied from the familiar reaction-diffusion-chemotaxis point of view in bacterial range expansion (11), marine (12) and more general ecological contexts (13), we suggest physical effects that go beyond that standard level of treatment (14). Chief among them is the way in which collective motion can act as a "thermal bath" in enhancing the diffusivity of suspended particles (15, 16), which in turn raises fundamental issues concerning generalizations of Fick's law (17, 18), particularly in the presence of hydrodynamic shear (19). Although studies of pattern formation in mixtures of motile and non-motile bacteria (20) and in mixtures of active and passive particles (21) have noted the contribution of activity-induced fluid flows to the spatial distribution of suspended tracers, our observations are distinct from those involving formation of crystallites of passive microspheres from the action of motile particles (22) and other types of light-switchable phenomena associated with Janus particles (23).

Our experiment to understand the dynamics of the ABC system involves a thin, quasi-two-dimensional suspension of non-motile algae and fluorescently labelled bacteria at initially uniform concentrations. As depicted in Fig. 1, a shaft of photosynthetically active light is cast on the suspension, triggering oxygen production by the illuminated algae. As shown in Figs. 2(a,b), this leads to chemotaxis of bacteria into the illuminated region, producing a high concentration of bacteria. Remarkably, we find that algae are then expelled from the illuminated region (see also SI Movie 1). Quantitative measurements of the local bacterial dynamics in the the system show that this expulsion is associated with a *gradient of bacterial concentration* from its peak at the center, leading to an outward algal transport. On longer time scales, after the algal expulsion, the bacterial concentration returns to uniformity as the bacteria diffusive outward in the absence of chemotactic stimulus. We name this *Type I* dynamics. Figures 2(c,d) show that at sufficiently high initial bacterial concentrations a new, *Type II* behavior is observed; expulsion of alga and consumption of oxygen are sufficiently rapid that many bacteria in the illuminated region become hypoxic, transition to an immotile state, and are then also expelled into the dark (see SI Movie 2).

We develop here a system of coupled PDEs for the dynamics of the ABC system that provides a quantitative account of the experimental observations. These PDEs incorporate diffusion, chemotaxis, oxygen production and consumption and algal transport by stochastic bacterial motion. The expulsion of algae has interesting similarities to the process known in magnetohydrodynamics (MHD) as "flux expulsion". First discovered for magnetic fields in a prescribed constant vortical flow field (24), in which field lines are expelled from the vortex, it was later recognized that this expulsion can arise from gradients in the intensity of turbulence whose random advection of the magnetic vector potential leads to a gradient in its effective diffusivity and thence to "turbulent diamagnetism" (25, 26). We show here that inclusion of advective contributions to the algal dynamics leads to a mathematical structure identical to that found in the flux expulsion problem, but involving the expulsion of a scalar quantity (the algal concentration) rather than a vector (the magnetic field in MHD).

Results

Figures 2 and 3 (along with SI Movies 1 and 2) summarize the main experimental observations associated with a homogeneous initial condition in darkness that is then illuminated with a shaft of light. The concentration of algae was fixed at

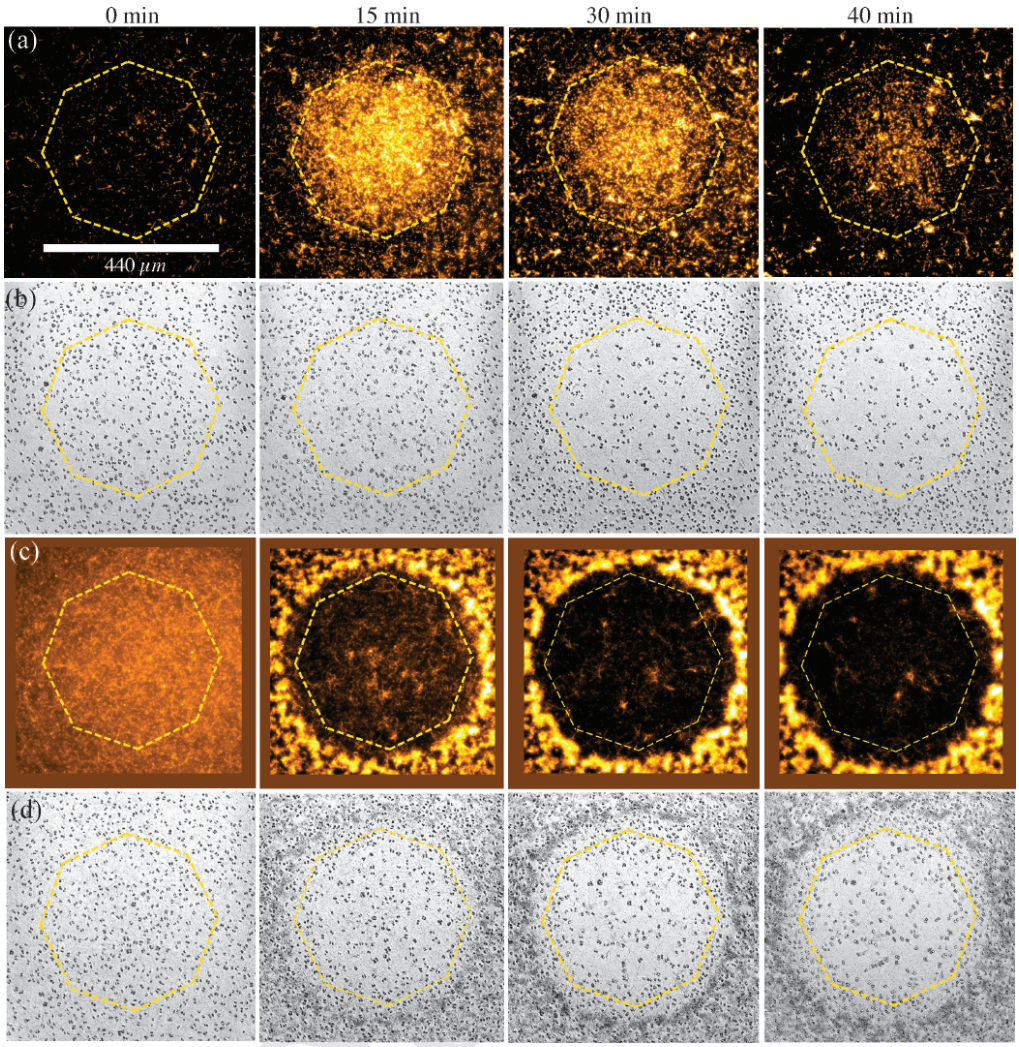

Fig. 2. Bacterial influx and algal expulsion. See SI Appendix, Figure S2 for additional examples of expulsion. (a) Type-I dynamics. Spatio-temporal evolution of bacterial concentration after illumination is initiated, where octagonal ring indicates boundary of illuminated region. At the low initial bacteria concentration ($\sim 1 \times 10^8$ cm^{-3}), bacteria first move into the illuminated region and then retreat. (b) Algal concentration as a function of time, demonstrating expulsion from illuminated region. (c) Type II dynamics. At a higher concentration ($\sim 5 \times 10^8$ cm^{-3}), many bacteria become non-motile and are expelled into the dark region, forming a concentrated circular accumulation that acts as a natural boundary. (d) Algae are also expelled, accumulating inside the confines of the bacterial accumulation.

5×10^6 cm^{-3} while varying the bacteria concentration in the range $(1-5)\times 10^8$ cm^{-3}. For an initial bacterial concentration of $b = 1 \times 10^8$ cm^{-3} giving Type I dynamics (SI Movie 1), we observe over the course of the first ~ 10 min after the start of illumination that the concentration of bacteria at the center of the illuminated region increases dramatically, as visualized in Fig. 2(a) and quantified in Fig. 3(a), reaching a peak enhancement of a factor of ~ 5, with a roughly linear decrease out to the edge. That peak then relaxes away until the bacterial concentration is again nearly uniform after ~ 35 min. At the peak of accumulation, after ~ 15 min, there is a clear bacterial depletion zone just outside the illuminated region, whose width is estimated to be $\sim 150\,\mu$m. During this period, as shown in Figs. 2(b) and 3(b), the algal concentration becomes strongly depleted within the illuminated region, with accumulation at its boundary.

We measured the mean squared displacement (MSD) of algae versus time at a range of radii r from the light shaft center. The MSD in Fig. 4(a) exhibits systematic upward curvature, with a local exponent of unity at time $t_1 \sim 6-7$ s, but faster behavior for $t > t_1$. Such superdiffusion for tracers is a well-known consequence of collective behavior in concentrated bacterial suspensions (9, 15). A heuristic illustration of the strong gradient in collective behavior in the illuminated region is obtained by determining an effective algal diffusion constant $\tilde{D}_a$ from the slope of the MSD curve at t_1 (inset of Fig. 4(a)), which is a strongly decreasing function of distance from the shaft center, that mirrors the decreasing bacterial concentration. The largest of these diffusivities is ~ 17 times the purely thermal value $D_{\rm th} = k_B T/6\pi\mu a \simeq 0.03\,\mu$m^2/s, where μ is the medium viscosity and $a = 6.5\,\mu$m is twice the algal radius since most algae exist as pairs ("palmelloids"). Yet, by itself, an effective algal diffusivity $\tilde{D}_a \sim 0.5\,\mu$m^2/s implies a diffusive time $R^2/\tilde{D}_a \sim 1600$ min for algae at the center to escape purely by random motion, far longer than the observed time of

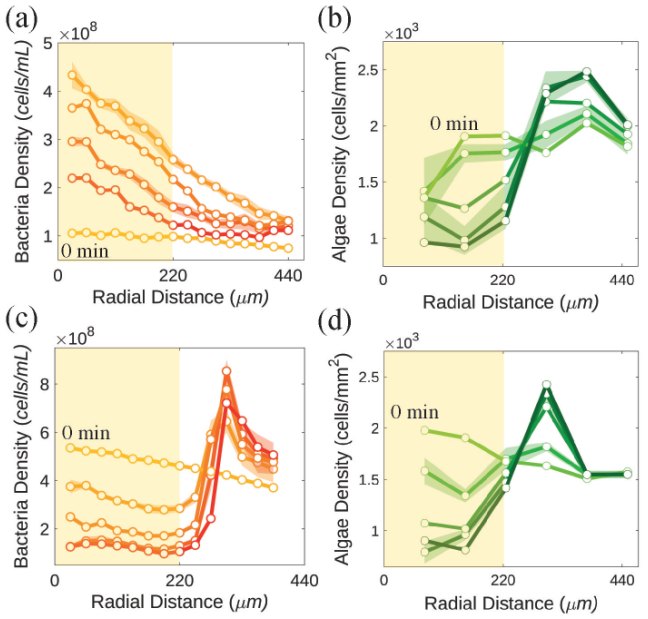

Fig. 3. Bacterial accumulation and algal expulsion. Yellow shading in the plots up to 220 μm indicates illuminated region. Standard error evaluated over the four quadrants is shown for 10 min and 30 min intervals. (a) Bacterial and (b) algal concentrations for a coculture with initial concentrations $b = 1 \times 10^8$ cm^{-3} and $a = 5 \times 10^8$ cm^{-3}, showing Type I dynamics. Shading of symbols and lines increase with time, with a ten minute interval between data sets. (c,d) As in (a,b) but with initial bacterial concentration $b = 5 \times 10^8$ cm^{-3}, exhibiting Type II dynamics.

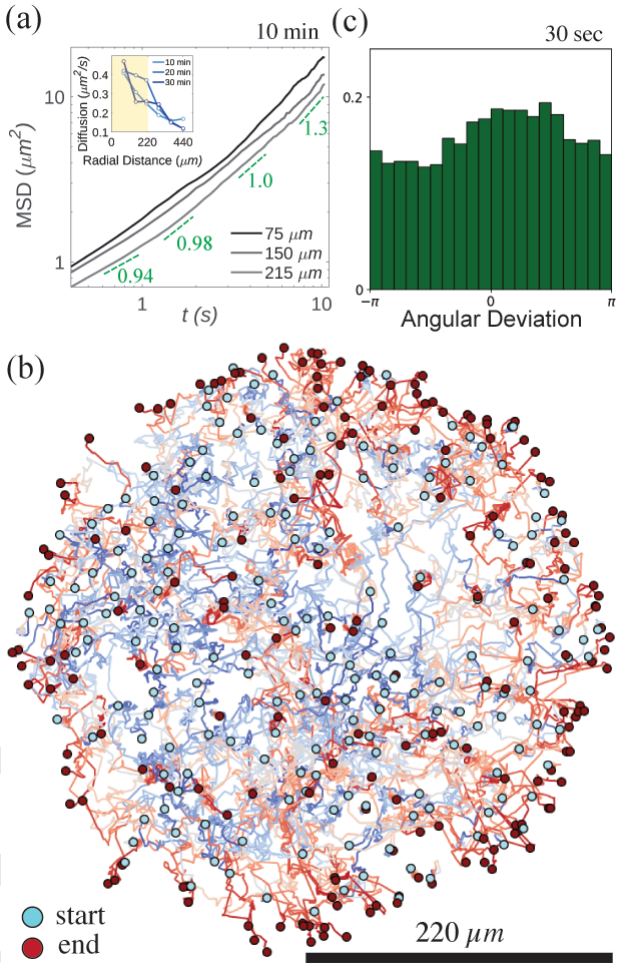

Fig. 4. Algal dynamics during expsulsion. (a) MSD of algae versus time for the cases shown in Fig. 3(a,b) at different radii in the illuminated region. Dashed lines indicate apparent slope at different times. Inset shows algal diffusivity determined in linear regime of MSD versus radial distance at various times after start of illumination. (b) Algal trajectories for Type I dynamics. Coloring along trajectories runs from blue (initial) to red (final) as algae are expelled from illuminated region. (c) Probability distribution of algal displacements for $\Delta t = 30$s as a function of angle with respect to the outward normal from the domain, illustrating peak in the outward direction.

30 min; the superdiffusive behavior seen for $t > t_1$ in Fig. 4(a) signals a distinct transport process. This conclusion is supported by capturing the trajectories of every algal cell within the illuminated region during the entire expulsion process, shown overlaid in Fig. 4(b) and in SI Movie 3. These trajectories are obtained at a sampling rate of 1 frame/s (fps). Subsampling them at larger time intervals gives insight into the angular distribution of displacements associated with interactions between bacteria and algae, as in the original notion of bacteria as a "bath" of particles analogous to the solvent molecules whose collisions with a tracer particle give rise to ordinary Brownian motion. Figure 4(c) shows those displacements for the time interval $\Delta t = 30$s, expressed as a function of the angle with respect to the outward normal from the domain at the location of each alga. We see a clear azimuthal nonuniformity with a peak in the outward direction. As the expulsion process occurs during the "retreat" of the bacteria from their initial chemotactic accumulation, this inhomogeneity in collisions is plausibly associated with the outward flow of bacteria.

At the higher initial bacterial concentration $b = 5 \times 10^8$ cm^{-3} we observe the distinct Type II behavior (SI Movie 2), as seen in Figs. 2(c,d) and 3(c,d): expulsion happens much more rapidly, the bacterial concentration profile becomes nonmonotic in radius, with a strong peak just outside the illuminated region, and the peak of the concentration of expelled algae is narrower. Close microscopic inspection of the region of high bacterial concentration in the dark region shows that most of the bacteria there are immotile and the expelled algae reside just inside the bacterial accumulation ring. We deduce that many bacteria in the illuminated region have become hypoxic and are expelled from that area through much the same process that expelled the algae. The algae in turn are confined by the ring of non-motile bacteria.

The ABC Model. We now turn to a mathematical model for the behavior described above, focusing first on Type I expulsion. In this case, a minimal description of the system entails the concentration fields $a(\mathbf{r}, t), b(\mathbf{r}, t)$ and $c(\mathbf{r}, t)$ for algae, bacteria, and oxygen, respectively. If D_c is the oxygen diffusion constant (assumed independent of all other variables), k_+ is the rate of oxygen production per algal cell when illuminated with a spatially varying light intensity $I(r)$ and the oxygen consumption rate per bacterium has a Michaelis-Menten form, then

$$c_t = D_c \nabla^2 c + k_+ a I(r) - k_- b \frac{c}{K_c + c}, \qquad [1]$$

where K_c is the Michaelis constant.

Consider first the situation of uniform illumination ($I = 1$) and uniform concentrations a_0 and b_0 of algae and bacteria.

A steady state $c^* = K_c k/(1-k)$, with $k = k_+ a_0/k_- b_0$, can be reached in which consumption balances production (see SI Appendix), provided $k < 1$. We assume this inequality is always satisfied and typically invoke the *weak production limit* $k \ll 1$, in which the oxygen consumption can be approximated as $k_- bc/K_c$.

We explain algal expulsion from the illuminated region through three intermediate calculations; oxygen production in a uniform suspension; bacterial chemotaxis in the presence of oxygen production; algal dynamics due to an inhomogeneous bacterial concentration. Suppose that the light is constrained to a shaft of radius R. Scaling time, space, and concentrations via $T = tD_c/R^2$, $\eta = r/R$, $\chi = c/c^*$, $\alpha = a/a_0$, and $\beta = b/b_0$, letting $\epsilon = k/(1-k)$, and introducing the *screening length*

$$\lambda = (D_c \tau_c)^{1/2}\,, \qquad [2]$$

where $\tau_c = K_c/k_- b_0$ is the characteristic consumption time of oxygen, the dynamics Eq. (1) takes the form

$$\chi_T = \nabla^2 \chi + (1-k)\kappa^2 \alpha \Theta(1-\eta) - \kappa^2 \beta \frac{\chi}{1+\epsilon\,\chi}, \qquad [3]$$

where now $\nabla^2 = \nabla^2_\eta$, and Θ is the Heaviside function. Here, $\kappa^2 = R^2/\lambda^2$ is also the ratio τ_D/τ_c of the time $\tau_D = R^2/D_c \sim 25\,\mathrm{s}$ for oxygen to equilibrate diffusively across the illuminated region to the consumption time.

If we clamp concentrations α and β at unity, take $k \ll 1$, and enforce continuity in χ and χ_η at $\eta = 1$, the steady state of Eq. (3) in an unbounded domain is

$$\chi(\eta) = \begin{cases} 1 - \kappa K_1(\kappa) I_0(\kappa\eta) & \eta \le 1, \\ \kappa I_1(\kappa) K_0(\kappa\eta) & \eta \ge 1, \end{cases} \qquad [4]$$

in terms of modified Bessel functions K_ν and I_ν. From the inner solution we see that the oxygen concentration at the centre of the illuminated region asymptotes to unity (c^* in unrescaled units) for large domain size κ, but is attenuated strongly as κ falls below unity. The outer solution behaves as $\chi \sim \exp(-(r-R)/\lambda)$, showing that λ is the penetration depth of oxygen into the surrounding bacterial population and sets the depletion zone seen in Fig. 1(b). With $D_c \sim 2\times10^3\,\mu\mathrm{m}^2/\mathrm{s}$ and $R = 220\,\mu\mathrm{m}$, and the estimate $\tau_c \sim 10^2\,\mathrm{s}$ (27), we find $\lambda \sim 400\,\mu\mathrm{m}$, and thus $\kappa \sim 1-2$.

Relaxing the assumption of uniform bacterial concentration, after a time τ_D bacteria within a distance λ of the edge of the illuminated region will experience the steepest oxygen gradient and chemotax most rapidly inwards. This can be described by the simplest combination of diffusion and chemotaxis as in the Keller-Segel model (28), $b_t = D_b \nabla^2 b - \boldsymbol{\nabla}\cdot(gb\boldsymbol{\nabla}c)$ where the diffusion constant D_b arises from random cellular swimming and the response coefficient g is taken to be constant. Scaling as above, we obtain

$$\beta_T = d\nabla^2\beta - \gamma\boldsymbol{\nabla}\cdot(\beta\boldsymbol{\nabla}\chi), \qquad [5]$$

where $d = D_b/D_c$, and $\gamma = gc^*/D_c$.

A steady state can be reached when the chemotactic flux $\gamma\beta\boldsymbol{\nabla}\chi$ balances the diffusive flux $d\boldsymbol{\nabla}\beta$, yielding

$$\beta_{ss}(\eta) = A\exp\left(\frac{\gamma}{d}\chi(\eta)\right), \qquad [6]$$

where A is a normalization constant. While this profile captures the observation that the bacterial concentration reaches its maximum at $\eta = 0$, where χ is maximized, the profile Eq. (6) only develops on time scales sufficient for bacteria outside the depletion zone to move inwards and replenish partially the depletion. This time will be at least $(R+\lambda)^2/D_b \gg \tau_D$. Prior to this the bacterial concentration is nonmonotonic, with the depletion zone seen in Fig. 2(a).

The flagella-less algae used in our experiments do not swim; their movement arises from collective flows driven by the concentrated bacteria. At the very least this leads to enhanced diffusivity, which, as seen in Fig. 3(f), varies in space, and by itself, is captured by an algal flux $\mathbf{J}_D = -\tilde{D}_a\boldsymbol{\nabla}a$. While this contribution is surely present, our observations of outward flux of alga from an initially uniform concentration suggest the growth of an unstable concentration mode during the depletion of algae, a phenomenon not captured by a purely diffusive term. In proposing a second contribution to the algal flux, we note that the algae will be advected by the local flows created by the swimming of the bacteria (15, 16, 29) and will be reoriented by collisions with them, where both effects will vary in space due to the gradients of bacterial concentration. In quantifying these effects we take motivation from classic work (17) on run-and-tumble locomotion in chemotaxis which considered situations in which the local swimming speed $\nu(\mathbf{x})$ and tumble rate $\omega(\mathbf{x})$ for an organism may vary with position $\mathbf{x}$. When the two are constant the organism density σ evolves via diffusion with a Fick's law flux $\mathbf{J} = -D\boldsymbol{\nabla}\sigma$, with a diffusion constant $D \propto \nu^2/\omega$. In the general case that both ν and ω vary there is an additional contribution to the flux proportional to $\sigma(\nu/\omega)\boldsymbol{\nabla}\nu$. Carrying this over to the algal dynamics, and assuming the simplest linear scalings $\nu \propto b$ and $\omega \propto b$, we obtain a contribution to the algal flux $\mathbf{J} = -pa\boldsymbol{\nabla}b$ for some $p > 0$. With the concentration seen in Fig. 3(a), whose radial gradient is negative, this contribution leads to an *outward* flux of algae.

Assembling these contributions and rescaling as above, we obtain two equivalent forms of the dynamics,

$$\alpha_T = \boldsymbol{\nabla}\cdot(d_a\boldsymbol{\nabla}\alpha) + \zeta\boldsymbol{\nabla}\cdot(\alpha\boldsymbol{\nabla}\beta)\,, \qquad [7a]$$

$$\alpha_T - \zeta\boldsymbol{\nabla}\beta\cdot\boldsymbol{\nabla}\alpha = \boldsymbol{\nabla}\cdot(d_a\boldsymbol{\nabla}\alpha) + \zeta\alpha\nabla^2\beta, \qquad [7b]$$

where $d_a = \tilde{D}_a/D_c$ and $\zeta = pb_0/D_c$. The first form Eq. (7a) shows a parallel to the bacterial chemotaxis equation Eq. (5); algae exhibit negative "bacteria-taxis". In the second form Eq. (7b), we see that there is an explicit advective contribution and a "reactive" term $\alpha\nabla^2\beta$. The latter is the sought-after linearly destabilizing term for a homogeneous initial algal concentration; it forces α down inside the illuminated region, whereupon it is advected outward.

Figures 5(a,b) show how the model defined by Eqs. 3, 5 and 7b provide a quantitative fit to Type I dynamics. In particular, we see the prompt accumulation of bacteria in the illuminated region followed by expulsion of algae. In the model and in experiment, the fraction of algae ultimately expelled is ~ 0.5, so there is still oxygen production within the illuminated region after $\sim 30\,\mathrm{min}$, leading to continued chemotactic attraction of bacteria inward. This leads to a slower decay of the bacterial concentration back to its original uniform, low value than seen in experiment. This may reflect processes such as bacterial adaptation to the oxygen and a gradual reduction in oxygen production by algae.

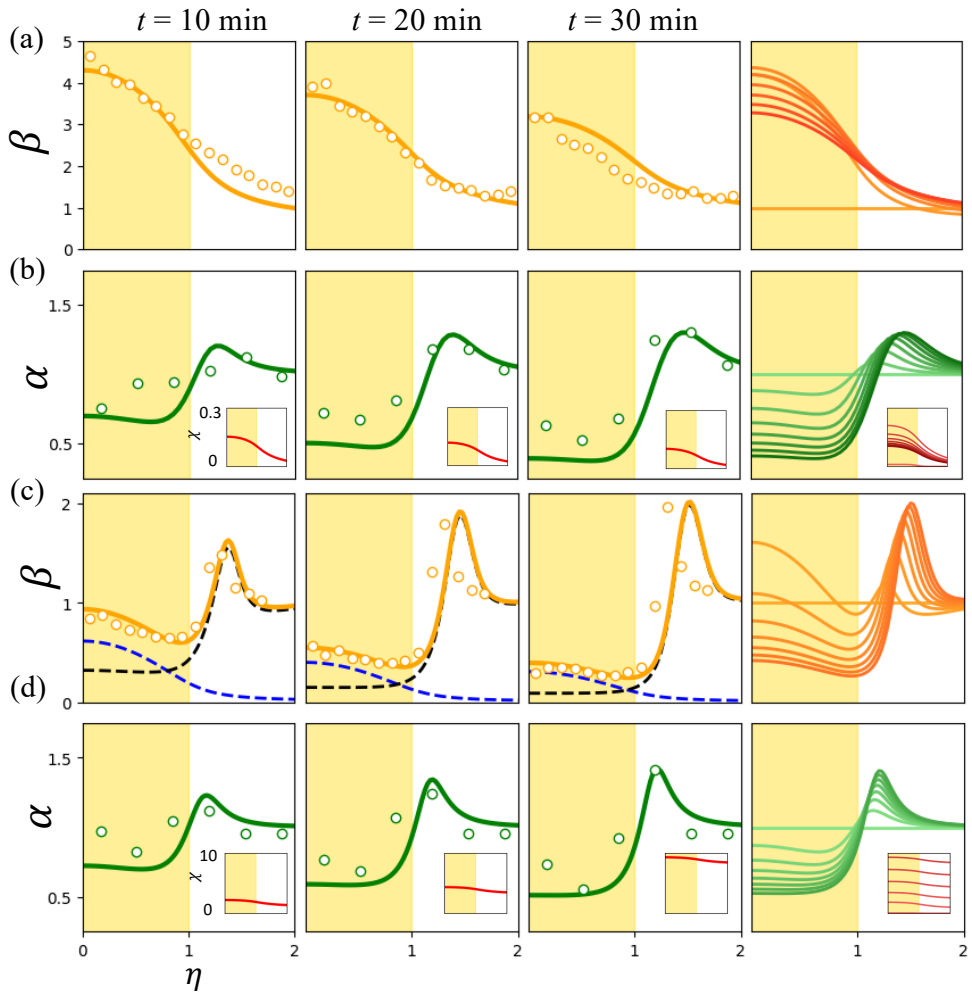

Fig. 5. Theoretical predictions. (a,b) Type I dynamics. (a) Non-dimensional bacterial dynamics from experiment (circles) compared to theoretical fit (solid lines) for first thirty minutes of experiment. Rightmost column in each row shows the theoretical time evolution over 30 minutes, sampled every ~ 3 minute. Shading intensity increases with time. (b) As in (a) but for algae, showing expulsion. Insets show theoretical oxygen profiles χ. (c,d) Type II dynamics. (c) Experimental bacterial dynamics (circles) compared to predictions of the ABCD model. Dashed lines indicate immotile (black) and active (blue) bacteria, whose sum is orange solid line. Rightmost plot shows time evolution of the total bacterial concentration. (d) Algal expulsion for high density experiment. For (a),(b) we took $\kappa^2 = 1, \epsilon = 1, d_b = 0.1, d_a = 0.0001, \gamma = 1.2, \zeta = 0.002$. For (c), (d), we use $\gamma = 0.35, \zeta = 0.005, \kappa^2 = 5, d_\delta = 10^{-4}, \rho = 1.0, \chi^* = 0.1, \zeta_d = 0.04, \delta^* = 0.01$ with all other parameter values held over.

The ABCD Model. While the ABC model can account for the essential features of Type I dynamics, it does not allow for loss of motility of bacteria at low oxygen concentrations in Type II dynamics. This transformation has been discussed in the context of bioconvection (27, 30), where influx of oxygen at the air-water interface of a bacterial suspension competes with consumption within the fluid, leading to a hypoxic region hundreds of microns below the surface. Hypoxia-induced motility transitions have also been observed in the penetration of oxygen into suspensions of *E. coli* (31).

To account for this transformation we view the "dormant", non-motile state of the bacteria, with concentration d, as a separate population distinct from the motile form, so the extended "ABCD" model involves algae, bacteria, chemoattractant, and dormant bacteria. The interconversion rate as a function of oxygen concentration c is taken as a simple generalization of the substrate-dependent growth of the Monod model, $v_{con} b K_{sat}/(c + K_{sat})$, where v_{con} is the maximum conversion rate to the immotile form and K_{sat} is the concentration at which half-maximal conversion occurs.

The dynamics of dormant bacteria include generation, expulsion, and a very small diffusion constant D_d. Setting $\delta = d/b_0$, the rescaled dynamics takes the form

$$\delta_T - \zeta_d \boldsymbol{\nabla}\beta \cdot \boldsymbol{\nabla}\delta = d_d \nabla^2 \delta + \zeta_d \delta \nabla^2 \beta + \rho\beta \frac{\chi^*}{\chi^* + \chi}, \quad [8]$$

where $d_d = D_d/D_c$, $\rho = v_{con} R^2/D_c$ and $\chi^* = K_{sat}/c^*$. Accordingly the bacterial dynamics Eq. (5) acquires the corresponding loss term from conversion, becoming

$$\beta_T = d\nabla^2 \beta - \gamma \boldsymbol{\nabla} \cdot (\beta \boldsymbol{\nabla}\chi) - \rho\beta \frac{\chi^*}{\chi^* + \chi}. \quad [9]$$

A final modification to the ABC model involves steric effects on algal diffusion that occur when the concentration of dormant bacteria is large. This is modelled by modifying the rescaled algal diffusivity d_a to $d_a(1 - \delta/(\delta + \delta^*))$, a form

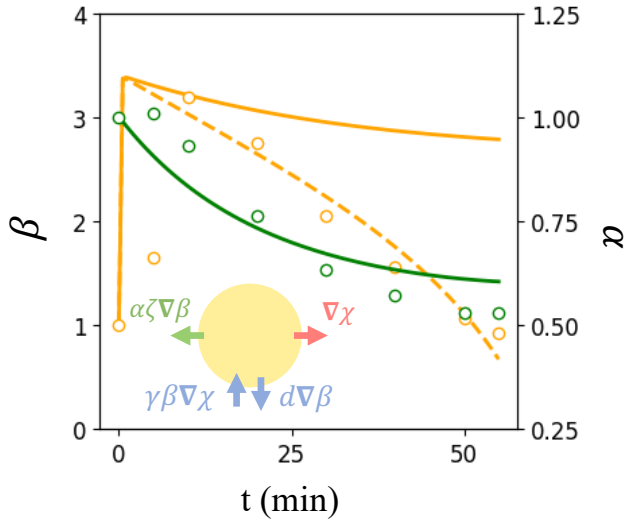

Fig. 6. Spatially averaged dynamics. Average concentration of bacteria (orange) and algae (green) in illuminated region from experiments (circles) and model (lines) shown in scattered points. For bacteria, simple chemotaxis is shown by solid orange line, adaptive chemotaxis shown dashed. Inset: Schematic of fluxes across the illuminated region.

that reduces d_a at large δ but retains its positivity. With these components, Fig. 5(c,d) show that the ABCD model captures the expulsion of both algae and immotile bacteria, with a narrow accumulation of dormant bacteria blocking transport of algae.

Spatially-averaged model. Insight into the basic process of algal expulsion can be obtained by constructing a spatially-averaged model which takes as dynamical degrees of freedom the mean concentrations of algae, bacteria, and oxygen inside the illuminated region, denoted by $\bar{\alpha}$, $\bar{\beta}$, and $\bar{\chi}$. As indicated schematically in Fig. 6, the specification of this averaged model requires estimates of the various fluxes across the boundary of the illuminated region. We anticipate that turbulent bacterial dynamics will homogenize oxygen inside the illuminated region, save for the area close to the boundary of width λ where the concentration rapidly decreases. From an integral form of Eq. (1) and the divergence theorem we have $\partial_t(\pi R^2\bar{c}) = -D_c \oint ds\hat{\mathbf{n}}\cdot\boldsymbol{\nabla}c$, where $\hat{\mathbf{n}}$ is the outward normal to the illuminated region. If we estimate $\hat{\mathbf{n}}\cdot\boldsymbol{\nabla}c \sim \bar{c}/\lambda$, then the PDE Eq. (1) becomes the ODE

$$\frac{d\bar{\chi}}{dT} = -2\kappa\bar{\chi} + (1-k)\kappa^2\bar{\alpha} - \kappa^2\bar{\beta}\frac{\bar{\chi}}{1+\epsilon\bar{\chi}}. \qquad [10]$$

Similar estimates hold for the averaged bacteria dynamics, where the relevant fluxes are the outward diffusive and inward chemotactic contributions. The diffusive contribution is precisely analogous to that for oxygen above. Since on the time scales of the experiment only bacteria within a distance λ outside the illuminated region sense the gradient, the inward Keller-Segel flux is also estimated as above, but with an upper limit on the bacterial concentration due to steric effects. This leads to the ODE version of Eq. (5),

$$\frac{d\bar{\beta}}{dT} = -2d\kappa\bar{\beta} + 2\gamma\kappa\left(\beta_{\max} - \bar{\beta}\right). \qquad [11]$$

Finally, the algae have an active flux $-pa\boldsymbol{\nabla}b$ that leads to expulsion, but there is little back-diffusion into the illuminated region. Yet, as algae accumulate at the boundary (Fig. 2), they form a thick ring that inhibits continued expulsion of algae. Introducing a saturation of the algal flux we obtain the ODE version of Eq. (7a),

$$\frac{d\bar{\alpha}}{dT} = 2\zeta\kappa\bar{\beta}\left(\alpha_{\max} - \bar{\alpha}\right). \qquad [12]$$

Using parameter values taken from Fig. 5 and fitting $\beta_{\max} \approx 5$ and $\alpha_{\max} \approx 0.5$, we obtain the solid green and orange curves shown in Fig. 6 for mean algal and bacterial concentrations in the illuminated region. The reduced model captures the slow exponential decay of the algal concentration, but while it reproduces the rapid bacterial influx in the first few minutes of the experiments, the predicted decay of the bacterial concentration, as remarked earlier for the full ABC model, is far slower than observations. The possibility that this discrepancy arises from adaptation of the bacteria to elevated oxygen levels can be explored by assuming a simple linear decay of the chemotactic coefficient, as $\gamma(T) = \gamma_0 - T/\tau$, where τ sets the adaptation rate. For $\tau = 1200$, the bacterial dynamics (dashed orange line in Fig. 6) matches closely with data, while the algal expulsion (not depicted) is essentially unchanged from the non-adaptive case.

Discussion

Connection with MHD. As our results suggest new phenomenology in active matter systems, it is instructive to return to the connection between algal expulsion and flux expulsion in magnetohydrodynamics. In the original case considered (24), a magnetic field in a fluid with velocity $\mathbf{u}$ obeys the Maxwell equation,

$$\mathbf{B}_t = \boldsymbol{\nabla}\times(\mathbf{u}\times\mathbf{B}) + D_m\nabla^2\mathbf{B}, \qquad [13]$$

where D_m is the magnetic diffusivity, and both $\mathbf{B}$ and $\mathbf{u}$ are taken to confined to the xy-plane. The magnitude of the magnetic vector potential $\mathbf{A} = A\hat{\mathbf{z}}$ then obeys the advection-diffusion equation

$$A_t + \mathbf{u}\cdot\boldsymbol{\nabla}A = D_m\nabla^2 A. \qquad [14]$$

With $\mathbf{u}$ a prescribed single-vortex velocity field, the initial condition $A = B_0 x$, corresponding to the space-filling uniform magnetic field $\mathbf{B} = \boldsymbol{\nabla}\times\mathbf{A} = -B_0\hat{\mathbf{y}}$, homogenizes inside the vortex, leaving $\mathbf{B} = 0$ zero there but A essentially undisturbed outside.

In the case of turbulent transport considered later (25, 26), it was shown that on long time and length scales the effect of the inhomogeneous turbulence is captured by an equation of motion for a vector potential component $\bar{A}$, averaged on those scales, of the form

$$\bar{A}_t = \boldsymbol{\nabla}\cdot\left(D^*\boldsymbol{\nabla}\bar{A}\right) \qquad [15]$$

where $D*$ is a turbulent diffusivity tensor. For the case in which the turbulence varies along one direction, say y, then the averaged x-component of the magnetic field $\mathcal{F} = \bar{B}_x$ obeys $\mathcal{F}_t = \nabla^2\left(D^*(y)\mathcal{F}\right)$, or

$$\mathcal{F}_t - 2(\partial_y D^*)\partial_y\mathcal{F} = D^*\nabla^2\mathcal{F} + \mathcal{F}\partial_{yy}D^*. \qquad [16]$$

This form has the same structure as our Eq. Eq. (7a), with the bacterial concentration β playing the role of the diffusivity tensor component. We conclude that the main difference between the two problems is the expulsion of a scalar (concentration) field in the present context compared to the expulsion of a vector quantity in MHD.

Implications for Active Matter. The results described here highlight the rich dynamical behavior that occurs in mixed active matter systems involving microorganisms from two Kingdoms of Life. While the dynamics of symbiosis is generally studied on time scales relevant to population dynamics or evolution (32–34), our findings indicate that short-term dynamics on the scale of minutes and hours can have a considerable impact on the spatial-temporal aspects of association, where chemotaxis and phenotypic switching dominate. Although we considered the simple case of light intensity that is piecewise constant, inhomogeneous activity arises. The treatment of such nonuniform active matter has received attention only recently, in the context of "invasion" (35) and active gels (36), but is central to any discussion of realistic ecologies. In this sense, generalizing the present setup to allow algal motility and phototaxis in the presence of an inhomogeneous light field may reveal even more striking dynamics when the oxygen sources are themselves motile.

Materials and Methods

The coculture used strain 168 of *B. subtilis* which was genetically engineered to express yellow fluorescent protein m-Venus with excitation at 515 nm and emission at 528 nm (37). A single bacterial colony was picked from an agar plate and grown overnight in Terrific Broth (TB) on an orbital shaker at 240 rpm and 30 °C. The bacteria intended for experiments were grown from overnight culture until exponential growth phase in Tris-min medium spiked with TB medium (Tris-min + 0.1 % w/v glycerol + 5 % w/v TB). The non-motile *C. reinhardtii* strain CC477 (*bld1-1*) was sourced from the Chlamydomonas Resource Center (38) and grown in Tris-min medium, on an orbital shaker at 240 rpm and 20 °C. The diurnal cycle was 12 h cool white light ($\sim 15\,\mu$mol photons/m^{2}s PAR), and 12 h in the dark.

Prior to experiments, bacteria and alga from their respective exponential growth phases were mixed in a modified Tris-min medium, with glycerol as a carbon source and bovine serum albumin to prevent cell adhesion (Tris-min + 0.1 % w/v glycerol + 0.01 % v/v BSA). The desired number density of cells was achieved by centrifugation at 4000 g. All cell concentrations and sizes were measured using a Beckman Coulter Counter (Multisizer 4e). The mixture of cells for each experiment was transferred to a glass cover slip chamber with a depth of 300 μm, separated by double-sided tape, and sealed airtight using UV glue. The chamber surfaces were passivated with PEG ($M_w = 5000$ g/mol).

Experiments were performed on a Nikon TE2000-U inverted microscope. The spatio-temporal variation in bacterial concentration was monitored by epifluorescence illumination with a $\times 20$ objective using a highly sensitive, back-illuminated camera (Teledyne Prime Σ 95B). Movies of algae cells were recorded through the brightfield channel using a Phantom V311 high-speed camera (Vision Research) at $\times 20$ magnification. The halogen lamp served as both a brightfield and photosynthetic light source. The size of a light shaft used to trigger photosynthesis was controlled by the field iris in the microscope condenser arm, producing an octogonal boundary in the focal plane with mean radius of $R = 220\,\mu$m. See SI Appendix for more experimental details.

Data, Materials, and Software Availability. Experimental data and analysis are here and source code for the model is here.

ACKNOWLEDGMENTS. We are grateful to Jim Haseloff for providing the fluorescent strain of *B. subtilis*, Kade Heckel for assistance in particle tracking and HPC, and to Kyriacos Leptos for numerous discussions. This work was supported by the Gordon and Betty Moore Foundation, Grant No. 7523 (PP & REG) and the U.K. Marshall Aid Commemoration Commission (YB).

1. T.W. Engelmann, Ueber Sauerstoffausscheidung von Pflanzenzellen im Microspectrum, Archiv für die gesamte Physiologie des Menschen und der Tiere **27**, 485-489 (1882).
2. G. Drews, Contributions of Theodor Wilhelm Engelman on phototaxis, chemotaxis, and photosynthesis, Photosynth. Res. **83**, 25–34 (2005).
3. R.E. Goldstein, Coffee stains, cell receptors, and time crystals: Lessons from the old literature, Phys. Today **71**, 32–38 (2018).
4. M.T. Croft, A.D. Lawrence, E. Raux-Deery, M.J. Warren, and A.G. Smith, Algae acquire vitamin B_{12} through a symbiotic relationship with bacteria, Nature **438**, 90–93 (2005).
5. F.J. Peaudecerf, F. Bunbury, V. Bhardwaj, M.A. Bees, A.G. Smith, R.E. Goldstein, and O. Croze, Mutualism Between Microbial Populations in Structured Environments: The Role of Geometry in Diffusive Exchanges, Phys. Rev. E **97**, 022411 (2018).
6. R. Stocker, J. R. Seymour, D. E. Hunt, M. F. Polz, Rapid chemotactic response enables marine bacteria to exploit ephemeral microscale nutrient patches, Proc. Natl. Acad. Sci. USA **105**, 4209-4214 (2008).
7. F.J. Peaudecerf, Ph.D. thesis, Mathematics, University of Cambridge (2017).
8. T.J. Pedley and J.O. Kessler, Hydrodynamic phenomena in suspensions of swimming microorganisms, Annu. Rev. Fluid Mech. **24**, 313-358 (1992).
9. C. Dombrowski, L. Cisneros, S. Chatkaew, J.O. Kessler, and R.E. Goldstein, Self-concentration and large-scale coherence in bacterial dynamics, Phys. Rev. Lett. **93**, 098103 (2004).
10. R.E. Goldstein, Green algae as model organisms for biological fluid dynamics, Annu. Rev. Fluid Dynamics **47**, 343–375 (2015).
11. J. Cremer, T. Honda, Y. Tang, J. Wong-Ng, M. Vergassola, and T. Hwa, Chemotaxis as a navigation strategy to boost range expansion, Nature **575**, 658–663 (2019).
12. H. Malchow, Spatio-temporal pattern formation in nonlinear non-equilibrium plankton dynamics, Proc. R. Soc. B **251**, 103–109 (1993).
13. R. Martinez-Garcia, C.E. Tarnita, and J.A. Bonachela, Spatial patterns in ecological systems: from microbial colonies to landscapes, Emerg. Top. Life Sciences **6**, 245–258 (2022).
14. J. Agudo-Canalejo and R. Golestanian, Active Phase Separation in Mixtures of Chemically Interacting Particles, Phys. Rev. Lett. **123**, 018101 (2019).
15. X.-L. Wu and A. Libchaber, Particle Diffusion in a Quasi-Two-Dimensional Bacterial Bath, Phys. Rev. Lett. **84**, 3017–3020 (2000).
16. K.C. Leptos, J.S. Guasto, J.P. Gollub, A.I. Pesci, and R.E. Goldstein, Dynamics of enhanced trancer diffusion in suspensions of swimming eukaryotic microorganisms, Phys. Rev. Lett. **103**, 198103 (2009).
17. M.J. Schnitzer, Theory of continuum random walks and application to chemotaxis, Phys. Rev. E **48**, 2553–2568 (1993).
18. A.W.C. Lau and T.C. Lubensky, State-dependent diffusion: Thermodynamic consistency and its path integral formulation, Phys. Rev. E **76**, 011123 (2007).
19. D. Leighton and A. Acrivos, The shear-induced migration of particles in concentrated suspensions, J. Fluid Mech. **181**, 415–439 (1987).
20. S.E. Burriel and R. Colin, Active Density Pattern Formation in Bacterial Binary Mixtures, PRX Life **2**, 023002 (2024).
21. J. Stürmer, M. Seyrich, and H. Stark, Chemotaxis in a binary mixture of active and passive particles, J. Chem. Phys. **150**, 214901 (2019).
22. D.P. Singh, U. Choudhury, P. Fischer, and A.G. Mark, Non-Equilibrium Assembly of Light-Activated Colloidal Mixtures, Adv. Matt. **29**, 1701328 (2017).
23. H.R. Vutukuri, M. Lisicki, E. Lauga and J. Vermant, Light-switchable propoulsion of active particles with reversible interactions, Nat. Comm. **11**, 2628 (2020).
24. N.O. Weiss, The Expulsion of Magnetic Flux by Eddies, Proc. R. Soc. A **293**, 310–328 (1966).
25. L. Biferale, A. Crisanti, M. Vergassola, and A. Vulpiani, Eddy diffusivities in scalar transport, Phys. Fluids **7**, 2725–2734 (1995).
26. L. Tao, M.R.E. Proctor, and N.O. Weiss, Flux expulsion by inhomogeneous turbulence, Mon. Not. R. Astron. Soc. **300**, 907–914 (1998).
27. I. Tuval, L. Cisneros, C. Dombrowski, C.W. Wolgemuth, J.O. Kessler, and R.E. Goldstein, Bacterial swimming and oxygen transport near contact lines, Proc. Natl. Acad. Sci. USA **102**, 2277-2282 (2005).
28. E.F. Keller and L.A. Segel, Model for chemotaxis, J. Theor. Biol. **30**, 225-234 (1971).
29. Y. Peng, L. Lai, Y.-S. Tai, K. Zhang, X. Xu, and X. Cheng, Diffusion of Ellipsoids in Bacterial Suspensions, Phys. Rev. Lett. **116**, 068303 (2016).
30. A.J. Hillesdon, T.J. Pedley, and J.O. Kessler, The development of concentration gradients in a suspension of chemotactic bacteria, Bull. Math. Biol. **57**, 299-344 (1995).
31. C. Douarche, A. Buguin, H. Salman, and A. Libchaber, *E. coli* and oxygen: A motility transition, Phys. Rev. Lett. **102**, 198101 (2009).
32. V. Piskovsky, N. Oliveira, Bacterial motility can govern the dynamics of antibiotic resistance evolution, Nature Communications **14**, (2023).
33. Y. Baig, H.R. Ma, H. Xu, L. You, Autoencoder neural networks enable low dimensional structure analyses of microbial growth dynamics, Nat Commun. **14**(1), 7937 (2023).
34. L. David, C. Maurice, R. Carmody, D. Gootenberg, J. Button, B. Wolfe, A. Ling, A. Devlin, Y. Varma, M. Fischbach, S. Biddinger, R. Dutton, P. Turnbaugh, Diet rapidly and reproducibly alters the gut microbiome, Nature **505**, (2013).
35. C.J. Miles, A.A. Evans, M.J. Shelley, and S.E. Spagnolie, Active matter invasion of a viscous fluid: Unstable sheets and a no-flow theorem, Phys. Rev. Lett. **122**, 098002 (2019).
36. R. Assante, D. Corbett, D. Marenduzzo, and A. Morozov, Active turbulence and spontaneous phase separation in inhomogeneous extensile active gels, Soft Matter **19**, 189–198 (2023).
37. P.J. Steiner, Ph.D. thesis, Plant Science, University of Cambridge (2017).
38. `https://www.chlamycollection.org/`

PNAS

Supporting Information for

Dynamics of an Algae-Bacteria Microcosm: Photosynthesis, Chemotaxis, and Expulsion in Inhomogeneous Active Matter

Praneet Prakash, Yasa Baig, François J. Peaudecerf and Raymond E. Goldstein

Corresponding Author: Raymond E. Goldstein.
E-mail: R.E.Goldstein@damtp.cam.ac.uk

This PDF file includes:

Supporting text
Figs. S1 to S3
Tables S1 to S2
Legends for Movies S1 to S3
SI References

Other supporting materials for this manuscript include the following:

Movies S1 to S3

Supporting Information Text

1. Overview of Experimental Design

Light illumination and cell phototoxicity. The algae-bacteria mixture was illuminated by a shaft of visible light ($R = 220\,\mu m$) from a broadband halogen lamp (OSRAM 64625 HLX - 100W 12V) that served both as a brightfield and photosynthetic light source. Before every experiment, the power of illuminated light within the octagonal light shaft was measured using a microscope slide power sensor (Thorlabs S170C) and maintained at $20\,\mu$W. This power is lower than the power in the diurnal chamber used for growing algae, where the algae are continuously illuminated for nearly 12 h during their growth phase. In comparison, the total experimental time is just 1 h, and thus algae cells remain completely viable.

Temperature control. All experiments were carried out in a temperature controlled environment maintained at 20°C. We placed the glass coverslip chamber on a circular stage, allowing maximal metallic contact around the illuminated region. The temperature was monitored for several hours using a 10kΩ NTC thermistor (sensitivity 0.1°C) affixed to the back of the device in the light path, with no change in temperature recorded. The illuminated volume is just $5\,\mu$L, compared to the total volume of upwards of $70\,\mu$L, facilitating the effective dissipation of heat from absorbed light. Additionally, a low cell volume fraction $\phi = 0.001$ allows nearly all light to pass through.

Availability of macronutrients (C, N, P). It is important to maintain the availability of macronutrients (N, P) during the experiment. The preferred medium for algae growth is Tris-min medium (1) and for the bacteria is Ordal's chemotaxis medium for *B. subtilis* (2), which is known to support bacterial motility for several hours. Tables S1 and S2 show the composition of Tris minimal medium and Ordal's chemotaxis medium for easy comparison; note that Tris minimal contains all the components of Ordal's chemotaxis medium. We use Tris minimal medium, with glycerol as a carbon source for our experiments (Tris-min $+\,0.1\%$ w/v glycerol $+\,0.01\%$ v/v BSA). This medium is preferred since it supports growth of algae up to $\sim 10^8\,\mathrm{cm}^{-3}$ and also sustains the bacterial motility for several hours. Before each experiment, the cells are introduced into the fresh medium where the number of algae cells is $\sim 5 \times 10^6\,\mathrm{cm}^{-3}$, which is much lower than the maximum number it can support.

Photosynthesis of *C. reinhardtii* and respiration of *B. subtilis*. The photosynthesis of organic carbohydrates by algae can be summarized (3) by the following reaction:

$$\mathrm{CO_2 + H_2O \xrightarrow{light} CH_2O + O_2} \qquad [1]$$

This is a simplistic representation and hides several other cellular processes (4). The typical consumption rate of CO_2 is $1 \times 10^{-7}\,\mu\mathrm{mol\,cells^{-1}\,h^{-1}}$ ($1.7 \times 10^7\,\mathrm{molecules\,cells^{-1}\,s^{-1}}$) and the production rate is O_2 is $0.5 - 1 \times 10^{-7}\,\mu\mathrm{mol\,cells^{-1}\,h^{-1}}$ ($0.85 - 1.7 \times 10^7\,\mathrm{molecules\,cells^{-1}\,s^{-1}}$) (5–8). Similarly, *B. subtilis* consumes O_2 and releases a proportional amount of CO_2. The uptake rate of O_2 is of the order of $5 \times 10^{-9}\,\mu\mathrm{mol\,cells^{-1}\,h^{-1}}$ ($8.5 \times 10^5\,\mathrm{molecules\,cells^{-1}\,s^{-1}}$) (9, 10). Therefore, in a mixture of light illuminated algae-bacteria, a competition exists between the production and consumption of O_2 and CO_2.

Algal activity without bacteria. The average size of algae cells is $13\,\mu$m with a thermal diffusion coefficient $0.03\,\mu\mathrm{m}^2/\mathrm{s}$. With such a low diffusivity, in the absence of bacteria that algae are essentially stationary on the time scale of the experiments, as shown in Fig. S1.

Bacterial activity without algae. When bacteria are introduced into the experimental chamber without algae, their speed at low cell concentrations ($\sim 1 \times 10^6\,\mathrm{cm}^{-3}$) remains nearly constant ($18 - 20\,\mu$m/s) during the experimental timescale (30 min). At higher concentrations, their activity eventually drops due to consumption of O_2. For $b \sim 1 \times 10^8\,\mathrm{cm}^{-3}$, it takes 20-25 minutes for motility to cease, while at $\sim 5 \times 10^8\,\mathrm{cm}^{-3}$ cells become immobile within 5 min.

2. Bacterial Influx and Algal Expulsion

Type I and Type II dynamics: O_2 and CO_2 production and consumption. In our experiments demonstrating Type I and Type II behavior, we maintained the algal concentration at $\sim 5 \times 10^6\,\mathrm{cm}^{-3}$ and bacteria concentration at $\sim 1 \times 10^8\,\mathrm{cm}^{-3}$ for Type I and $\sim 5 \times 10^8\,\mathrm{cm}^{-3}$ for Type II dynamics. Slight variations in the exact number of cells across different repeats (Figs. S2 & S3) are due to the nature of centrifugation and mixing. At lower bacteria concentrations $\sim 5 \times 10^7\,\mathrm{cm}^{-3}$, the influx of bacteria into the illuminated region is very weak and does not lead to algal expulsion within the experimental timescale. While at the higher concentration of $\sim 1 \times 10^9\,\mathrm{cm}^{-3}$, ambient O_2 levels become insufficient to sustain bacterial motility.

From direct experimental observation, we have seen that bacterial motility without algae ceases within 20 mins for $b \sim 1 \times 10^8\,\mathrm{cm}^{-3}$ and within 5 mins for $b \sim 5 \times 10^8\,\mathrm{cm}^{-3}$. Clearly, oxygen is a limiting factor and as explained in Section 1 above, the O_2 production rate of *C. reinhardtii* is 100 times the consumption by *B. subtilis* on a per cell basis. Thus, if the number of bacteria is nearly 100 times that of algae, a competition between production and consumption of O_2 will be established. This is observed in Type I ($b/a = 50$) and Type II ($b/a = 100$) dynamics. For CO_2, as a first approximation we note that its dissolved concentration in fresh water is 38 mM (11), which translates to a total $\sim 1.7 \times 10^{-9}$ mole ($\sim 1 \times 10^{15}$ molecules) in the illuminated region. There are $\sim$ 300 cells in the illuminated region and they consume at most $\sim 3 \times 10^{-11}$ mole ($\sim 1.8 \times 10^{12}$ molecules) during the experimental timescale of 1 hr. Further, in Type I case, at the start of experiment bacteria influx proves that there is sufficient CO_2 concentration for normal algal metabolism. Over time the concentration of bacteria further increases, that will lead to even higher CO_2 availability in the illuminated region. Hence, there is sufficient CO_2 and the dynamics is solely governed by O_2 dynamics.

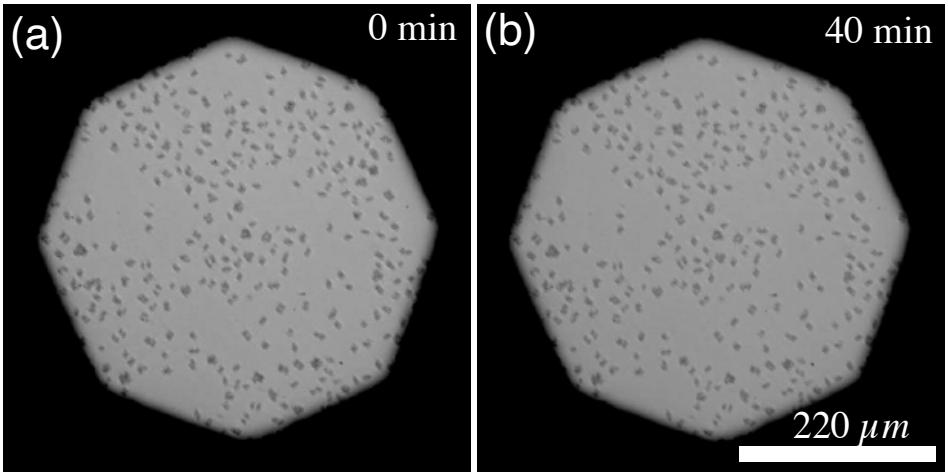

Fig. S1. Test for the effects of light on the algal distribution. (a) Initial distribution ($a = 4 \times 10^6\ \mathrm{cm}^{-3}$). (b) After 40 minutes of continuous illumination there is no discernable change in the spatial distribution.

Table S1. Tris minimal medium

Species	Na^{+}	K^{+}	Mg^{2+}	Ca^{2+}	SO_4^{2-}	NH_4^{+}	PO_4^{3-}	$EDTA^{4-}$
Molarity	312 μM	1.72 mM	410 μM	340 μM	0.41 mM	7.5 mM	1 mM	150 μM
Species	$H_2BO_3^{-}$	Mn^{2+}	Cu^{2+}	MoO_4^{2-}	Co^{2+}	Zn^{2+}	Fe^{2+}	Tris
Molarity	18 μM	76.5 μM	180 μM	25.8 μM	6.4 μM	6.3 μM	6.7 μM	20 mM

Table S2. Ordal's chemotaxis medium

Species	Na^+	K^+	Ca^{2+}	SO_4^{2-}	NH_4^+	PO_4^{3-}	$EDTA^{4-}$	Cl^-	lactate
Molarity	5 mM	10 mM	140 μM	300 μM	600 μM	10 mM	100 μM	280 μM	5 mM

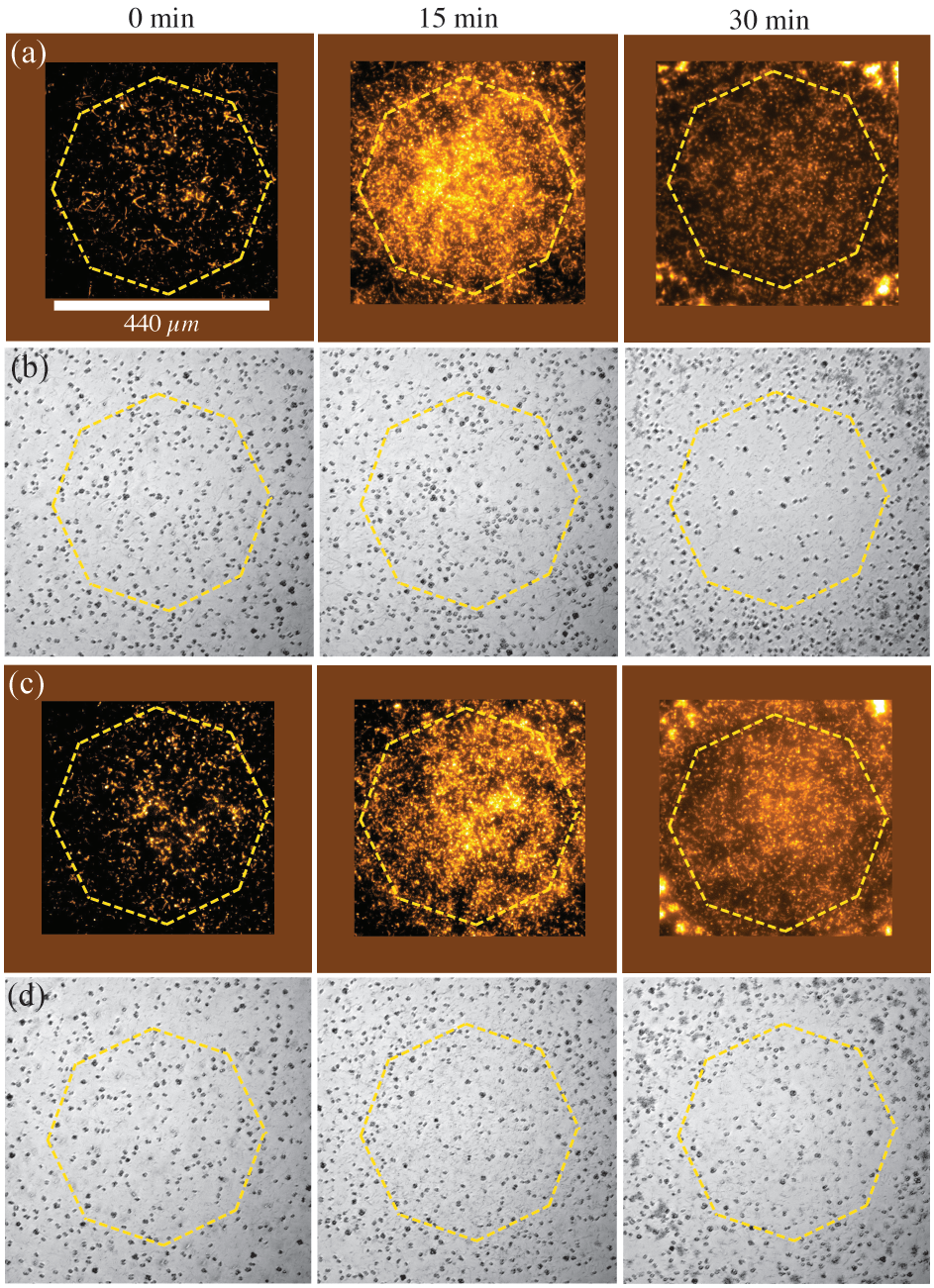

Fig. S2. Repeats of Type I algal expulsion. (a,b) $a = 6 \times 10^6$ cm^{-3}, $b = 1.5 \times 10^8$ cm^{-3}. (c, d) $a = 4 \times 10^6$ cm^{-3}, $b = 1.3 \times 10^8$ cm^{-3}.

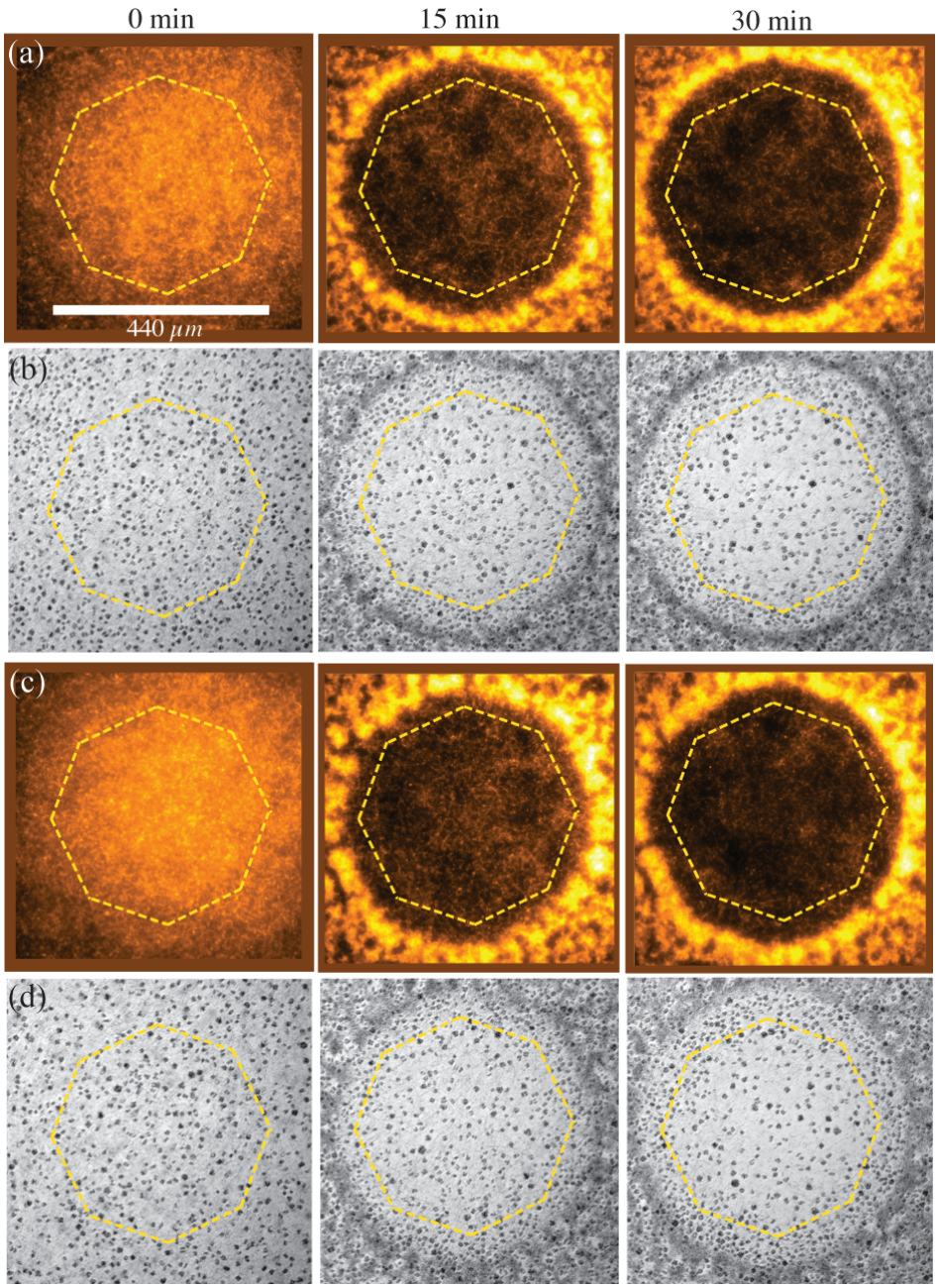

Fig. S3. Repeats of Type II algal expulsion. (a,b) $a = 6.5 \times 10^6$ cm^{-3}, $b = 4.3 \times 10^8$ cm^{-3}. (c, d) $a = 6.5 \times 10^6$ cm^{-3}, $b = 5.0 \times 10^8$ cm^{-3}.

Movie S1. Movie illustrating Type I algal expulsion. Fluorescence and brightfield video of bacteria and algal dynamics under continuous illumination by a shaft of photosynthetic light extending from the centre of the images up to 440 μm. The concentration of algae was 5×10^6 cm^{-3} while that of bacteria was 1×10^8 cm^{-3}.

Movie S2. Movie illustrating Type II algal expulsion. Fluorescence and brightfield video of bacteria and algal dynamics under continuous illumination by a shaft of photosynthetic light extending from the centre of the images up to 440 μm. The concentration of algae was 5×10^6 cm^{-3} while that of bacteria was 5×10^8 cm^{-3}.

Movie S3. Movie showing Type I expulsion of algae. Segmented video shows algae being expelled radially outward from the illuminated region as time progresses.

References

1. https://www.chlamycollection.org/.
2. G.W. Ordal and K.J. Gibson, Chemotaxis toward amino acids by *Bacillus subtilis*, J. Bacteriol. **129**, 151–155 (1977).
3. *The Chlamydomonas Source Book: Organellar and Metabolic Processes*, Vol. 2, A.R. Grossman and F.-A. Wollman, eds. (Academic Press, 2023).
4. M.R. Badger, Photosynthetic Oxygen Exchange, Annu. Rev. Plant Physiol. **36**, 27–53 (1985).
5. P. Vance and M.H. Spalding, Growth, photosynthesis, and gene expression in *Chlamydomonas* over a range of CO_2 concentrations and CO_2/O_2 ratios: CO_2 regulates multiple acclimation states, Canad. J. Bot. **83**, 796–809 (2005).
6. D. Sultmeyer, K. Klug and H. Flock, Effect of dissolved inorganic carbon on oxygen evolution and uptake by *Chlamydomonas reinhardtii* suspensions adapted to ambient and CO_2-enriched air, Photosynth. Res. **12**, 25–33 (1987).
7. G. Peltier and P. Thibault, Light-Dependent Oxygen Uptake, Glycolate, and Ammonia Release in L-Methionine Sulfoximine-Treated *Chlamydomonas*, Plant Physiol. **77**, 281–284 (1985).
8. A. Kaplan and J.A. Berry, Glycolate Excretion and the Oxygen to Carbon Dioxide Net Exchange Ratio during Photosynthesis in *Chlamydomonas reinhardtii*, Plant Physiol. **67**, 229–232 (1981).
9. L.S. Wong, M.S. Johnson, I.B. Zhulin and B.L. Taylor, Role of methylation in aerotaxis in *Bacillus subtilis*, J. Bacteriol. **177**, 3985–3991 (1995).
10. A.J. Hillesdon, T.J. Pedley and J.O. Kessler, The development of concentration gradients in a suspension of chemotactic bacteria, , 57, 299-344, 1995. Bull. Math. Biol. **57**, 299–344 (1995).
11. J.A. Dean, *Lange's Handbook of Chemistry*, 15$^{\text{th}}$ edition (McGraw Hill, 1999).